

High-Q cavity coupled to a high permittivity dielectric resonator for sensing applications

Shahnam Gorgi Zadeh,^{1,*} Alberto Ghirri,^{2,†} Sergio Pagano,³ Simone Tocci,⁴ Claudio Gatti,⁴ and Antonio Cassinese⁵

¹*European Organization for Nuclear Research (CERN), Meyrin 1217, Switzerland*

²*Istituto Nanoscienze - CNR, Centro S3, via G. Campi 213/A, 41125, Modena, Italy*

³*Physics Department, University of Salerno and INFN GC Salerno,
via Giovanni Paolo II 132, Fisciano (SA), Italy*

⁴*INFN, National Institute for Nuclear Physics, I-00044, Frascati, Italy*

⁵*Physics Department and INFN -Napoli, Università Napoli Federico II, P.le Tecchio 80, 80125 Naples, Italy*

The use of high quality factor resonators is of undoubted interest for high precision measurements and for applications in quantum technologies. Novel types of microwave sensors can be realized by coupling a first resonator acting as a stable frequency reference with a second resonator that is sensitive to a particular physical quantity. Here we report on a coupled cavity configuration in which a high Q -factor elliptical TESLA-shaped superconducting cavity is coupled with a high permittivity (ϵ_r) SrTiO₃ puck, whose resonant frequency varies as a function of temperature due to the temperature dependence of the permittivity that reaches values higher than 30000 below 1 K. Extensive electromagnetic simulations are used to test different coupling configurations, showing great versatility to tune the coupling in the weak or strong regime, depending on the puck's position within the cavity. Moreover, for the coupled system, they allow one to investigate the dependence of the zero transmission frequency value on changes of the permittivity ϵ_r , obtaining a maximum value of 2.8 MHz per unit change of ϵ_r , for $\epsilon_r \approx 230$. Finally, we discuss a specific application of the coupled system as a bolometer in different temperature ranges.

I. INTRODUCTION

Resonant cavities, with their ability to sustain high electromagnetic fields, have emerged as powerful tools for ultra-sensitive measurements. These structures, also known as resonators, operate by confining electromagnetic waves within a bounded region, allowing for resonance at specific frequencies. The high-quality factors (Q -factors) associated with resonant cavities provide high sensitivity, and thus potential high measurement precision and accuracy for the measurements of different physical quantities, making them indispensable in various scientific and engineering applications.

The use of resonant cavities for sensitive measurements has a rich history, particularly in the fields of fundamental physics, metrology, and quantum mechanics. In the field of particle physics, high- Q microwave cavities have been instrumental in the search for axions, hypothetical particles proposed as dark matter candidates [1, 2]. Similarly, resonant cavities are used in experiments testing the fundamental constants of nature, providing critical tests of physical theories beyond the Standard Model [3–5]. In quantum information science, superconducting microwave cavities are employed to couple qubits and facilitate quantum state readout with high fidelity [6, 7]. Furthermore, hybrid quantum systems combining resonant cavities with other quantum technologies, such as optomechanical or spin systems such as nitrogen-vacancy centers in diamond, have shown promise for enhanced

sensitivity in detecting weak forces and fields. These hybrid systems leverage the strong coupling between cavity modes and quantum states to achieve unprecedented measurement sensitivity [8]. The inherent sensitivity of resonant cavities also extends to applications in precision spectroscopy and time-keeping [9–11].

The coupling of two, or more, resonators has been exploited for several of the above-mentioned applications [12–17]. If a high Q factor resonator provides a stable reference frequency, the coupling with a second resonator can be used as an additional resource and to make the system sensitive to a specific physical quantity. For example, superconducting cavities were coupled in different ways showing that the photon lifetime of the local field can exceed that of the bare cavities [18]. Coupled sapphire resonators showed increased Q -factor and tunability due to the supermode effect, which was studied for axion detection with high sensitivity [19]. Moreover, systems composed of coupled dielectric resonators were investigated for the bolometric detection of particles and X-ray photons [12, 20–22]. There, a sapphire resonator acting as a stable reference frequency is coupled to a second resonator having a strongly temperature-dependent permittivity (e.g. CaTiO₃ or SrTiO₃). The absorption of energy causes a change in the absorber's permittivity, in turn producing a measurable change in the resonant frequency of the coupled system. Additionally, coupled resonator systems typically show a transmission zero, or notch, at the frequency for which the injected power is completely reflected back. The notch frequency and depth are sensitive probes of the frequency and coupling of the resonant modes [17, 23, 24].

Dielectric resonators have attracted long time inter-

* shahnam.zadeh@uni-rostock.de

† alberto.ghirri@nano.cnr.it

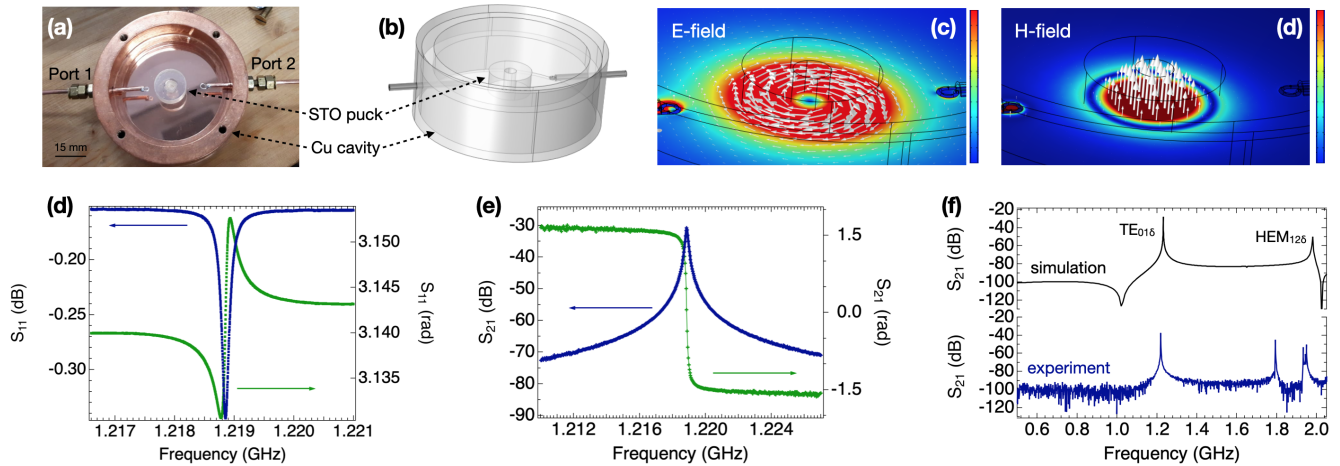


FIG. 1. Characterization of the STO resonator at room temperature. (a) Photograph showing the STO puck and Cu cavity used in the experiments. (b) Sketch of the model used for simulations (COMSOL Multiphysics). The top cap is not shown. (c,d) Simulated distribution of the root-mean-square electric and magnetic field for the TE_{015} mode ($\epsilon_r = 318$). (d,e) Plots of reflection (S_{11}) and transmission spectra (S_{21}) measured at room temperature (incident power 0 dBm). The amplitude is shown in blue, the phase in green. (f) Comparison between simulated and experimental S_{21} spectra. The peak at 1.22 GHz is reproduced by the simulated TE_{015} mode, while the dip displayed by the simulation at ≈ 1 GHz is below the background transmission of the cavity (-100 dB). The peak at 1.8 GHz is probably related to the hybrid HEM_{126} mode, although in this case the simulation shows a mismatch of ≈ 200 MHz.

est for several applications in sensing, metrology and detectors due to their well defined resonant modes and high Q -factors. High permittivity materials such as $SrTiO_3$, $KTaO_3$, $LaAlO_3$ and TiO_2 have been used in different situations, including room-temperature masers [25], dark matter searches [26] quantum sensing [27] and spin manipulation [28]. In particular, strontium titanate ($SrTiO_3$) has been the subject of intense study because of its peculiar physics [29], characterized in particular by quantum paraelectricity [30–32] and superconductivity [33] at low temperature, multiferroicity [34] and emergent conductivity or magnetism at the interface with other oxides, i.e. in $LaAlO_3/SrTiO_3$ heterostructures [29]. The properties of $SrTiO_3$ at microwave frequencies were also investigated [35–37], recently reporting also the anomalous behavior of complex permittivity below 1 K [38, 39].

Here we focus on the investigation of a particular system of coupled resonators, in which a strontium titanate (hereafter STO) puck is placed in a three-dimensional elliptical cavity. The latter specifically corresponds to a superconducting TESLA cavity at 1.3 GHz, whose geometry has been developed in the context of particle accelerators to obtain Q -factors as high as 10^9 [40]. We first characterize the STO resonator alone and test the evolution of permittivity and losses at temperatures down to 150 mK. We then exploit finite-element electromagnetic simulations to study the coupling between elliptical cavity and dielectric resonator, discussing the tuning of frequency and Q -factor of the coupled modes as a function of geometric and material parameters, such as the position of the STO puck within the cavity and the permittivity of the STO puck. These results demonstrate

great tunability for the proposed coupled system and allow the definition of conditions to control the coupling between high- Q cavities and high permittivity dielectric resonators, opening a path for the exploitation of these systems in applications. In particular, we discuss the exploitation of coupled cavity-STO resonator system for the realization of bolometers working in different temperature ranges.

II. CHARACTERIZATION OF THE STO RESONATOR

The dielectric resonator was realized with a STO crystal produced by SurfaceNet GmbH that was shaped into a cylinder having radius $a=8.17$ mm and height $d=7.26$ mm, with a central hole of radius 2 mm. For the characterization of the dielectric resonator we used a hollow copper cavity (inner radius 60 mm, height 22 mm), whose lowest mode at 3.8 GHz stands well above the fundamental mode of the dielectric resonator in order to avoid cross couplings between their modes. The STO puck was installed on top of two quartz spacers and coupled to the coaxial lines by loop antennae positioned at a distance of 10-20 mm from the outer surface of the cylinder (Fig. 1(a)). Measurements were carried out with the whole set-up installed either at room temperature, in liquid nitrogen or in a dilution fridge.

Room temperature measurements. Reflection and transmission spectra acquired at room temperature show the fundamental mode of the STO resonator at frequency $f_0 = 1.22$ GHz (Fig. 1(d,e)). Considering the geomet-

ric factors of the resonator and the STO permittivity $\epsilon_r \approx 318$, we obtain that f_0 corresponds well with the frequency of the $TE_{01\delta}$ mode derived by the semi-analytical formula [41]

$$f_{STO} \approx \frac{\alpha}{\sqrt{\epsilon_r}} \quad (1)$$

being $\alpha[\text{GHz}] = 34/(a[\text{mm}]) (a/d + 3.45)$, while a and d are the radius and height of the puck, respectively. The loaded quality factor extracted from the transmission spectrum (Fig. 1(e)) is $Q_L = 8000$. Since the loops are positioned far apart from the dielectric puck, the small coupling between feedlines and resonator turns into insertion loss of 30 dB. Thus, the internal quality factor can be approximated as $Q_0 \approx Q_L \approx 1/\tan \delta$. The loss tangent of STO results $\tan \delta = 1.2 \times 10^{-4}$. Finite-element electromagnetic simulations confirm the distribution expected for the $TE_{01\delta}$ mode (Fig. 1(c,d)), whose frequency results about 1.2 GHz in close agreement with experimental data (Fig. 1(f)).

Low temperature behavior. The temperature evolution between 4 and 300 K of cylindrical STO resonators is reported in the literature [35–37]. In this temperature range, the maximum Q -factor value of 20000 is reached around 100 K, just above the structural temperature transition of STO. The nonlinear change in the permittivity of STO encompasses two orders of magnitude to obtain $\epsilon_r \approx 3 \times 10^4$ and $\tan \delta \approx 1 \times 10^{-4}$ at 5 K [35].

We have tested the STO resonator at temperatures below 1 K (Fig. 2). The STO resonator was slowly cooled down to 150 mK in about 6 hours. The temperature was measured using a thermometer installed into the copper cavity. At the lowest temperature, the $TE_{01\delta}$ mode frequency resulted $f_0 = 116.9$ MHz with $Q \approx 1 \times 10^4$; these values suggest $\epsilon_r \approx 3 \times 10^4$ and $\tan \delta \approx 1 \times 10^{-4}$. As a function of the decreasing temperature, the frequency of the $TE_{01\delta}$ mode decreases until 0.4 K, while for lower temperatures we observe a slight upturn. In this temperature (T) range, the frequency of the resonator can be reproduced using a polynomial curve, $f_{STO} = K_0 + K_1T + K_2T^2$. The fit of the experimental points (Fig. 2(b)) gives $K_0 = 116.88$ MHz, $K_1 = -0.008$ MHz/K and $K_2 = 0.012$ MHz/K².

III. COUPLED STO AND ELLIPTICAL CAVITY

This section examines the coupling of the STO puck with a resonating cavity to form a coupled resonator system. To facilitate this investigation, we selected an elliptical TESLA-shaped cavity[40] operating at 1.3 GHz. This frequency was selected because it closely matches the operational frequency of the available STO puck sample at room temperature and because similar elliptical cavity prototypes were available for measurement at the European Organization for Nuclear Research (CERN). However, it is important to emphasize that the choice of

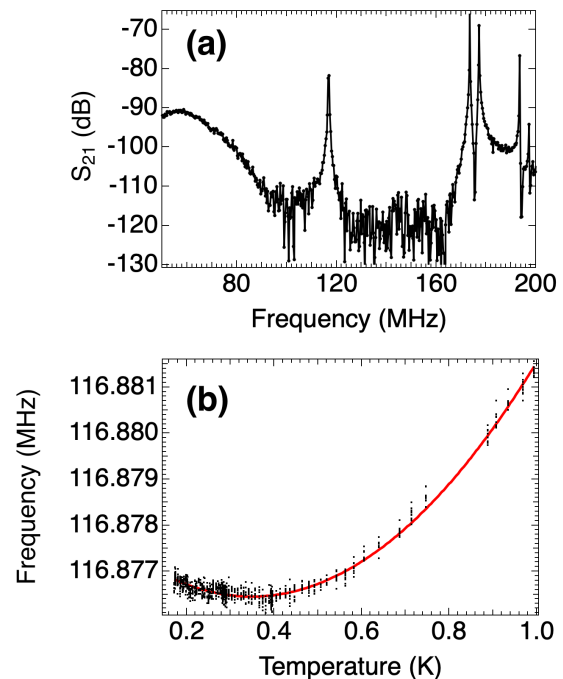


FIG. 2. Characterization of the STO resonator at temperature below 1 K. (a) Transmission spectrum acquired at 170 mK. (b) Temperature dependence of the fundamental mode frequency. The red solid line shows the fit of the experimental points

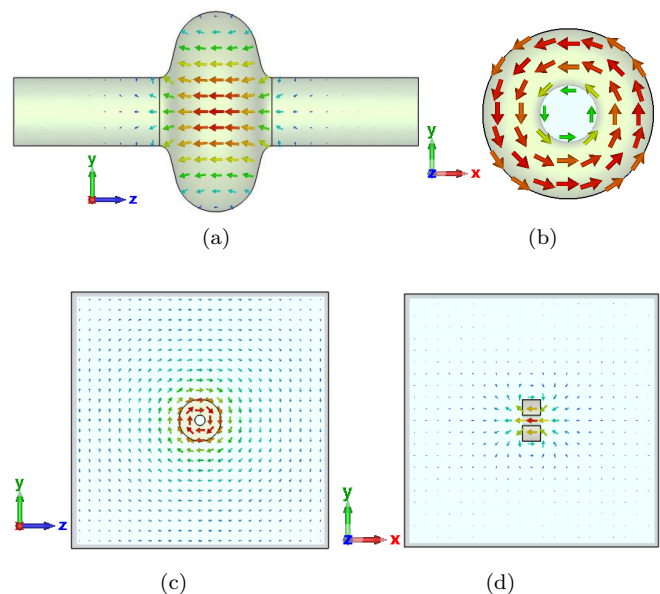


FIG. 3. Field distributions for the TM_{010} mode in a TESLA-shaped 1.3 GHz accelerating cavity: (a) electric field and (b) magnetic field. Additionally, field distributions for the first mode of the STO puck: (c) electric field and (d) magnetic field.

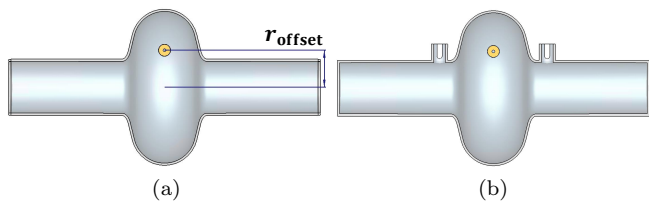


FIG. 4. Simulation setups of the coupled elliptical cavity and STO puck. The radial offset of the STO puck (r_{offset}) influences the coupling strength between the two modes. (a) Eigenmode analysis setup, and (b) S-parameter analysis setup.

cavity and frequency is not limited to the elliptical cavity at 1.3 GHz; other cavity types and frequencies may be used based on specific project requirements. The primary aim of this study is to assess the feasibility of coupling between the STO puck and a superconducting RF cavity.

Electromagnetic simulations. The TESLA-shaped elliptical cavity and its fundamental mode (FM), which is a transverse magnetic (TM) mode, are illustrated in Fig. 3. The cavity's equator radius was adjusted to achieve a frequency of 1.3 GHz. For a copper cavity, the quality factor of this mode at room temperature is 2.89×10^4 . By assuming $\epsilon_r = 318$, the first mode of the STO puck has a frequency of 1.10 GHz and a quality factor of 1.01×10^4 . The field plot of this mode is also shown in Fig. 3. The eigenmode and frequency domain simulations in this section were performed using CST Studio Suite.

To investigate the coupling between the two modes, the STO puck is placed inside the elliptical cavity. Two essential parameters for effective coupling are the orientation of the STO puck within the elliptical cavity and its radial offset from the center. The puck's position in the elliptical cavity for effective coupling is shown in Fig. 4. Coupling is examined using both eigenmode analysis and frequency domain analysis, with two identical antennas, each having $Q_{\text{ext}} = 8.6 \times 10^7$. In the eigenmode analysis, no antennas are considered, and the only losses accounted for are the dielectric losses of STO and surface losses on the elliptical cavity if non-perfect electric conductor (PEC) materials are used.

The results of the eigenmode analysis are presented in Fig. 5. The investigation examines how varying ϵ_r of the STO, which can be a function of temperature, affects the resonant frequency and Q -factor of the first two modes in the coupled system. The STO-dominant mode is characterized by having most of its energy localized in the STO, while the elliptical cavity-dominant mode retains most of its energy within the elliptical cavity, similar to the uncoupled system. Below $\epsilon_r = 230$, Mode 2 is the STO-dominant mode and Mode 1 is the elliptical cavity-dominant mode. Above $\epsilon_r = 230$, the order of the modes is reversed. When $r_{\text{offset}} = 0$ mm, the two modes do not interact as ϵ_r changes. In this scenario, the elliptical cavity's frequency (Fig. 5(a)) and Q -factor (Fig. 5(b)) remain nearly constant at 1.3 GHz and $Q_{\text{ext}} = 4.2 \times 10^7$,

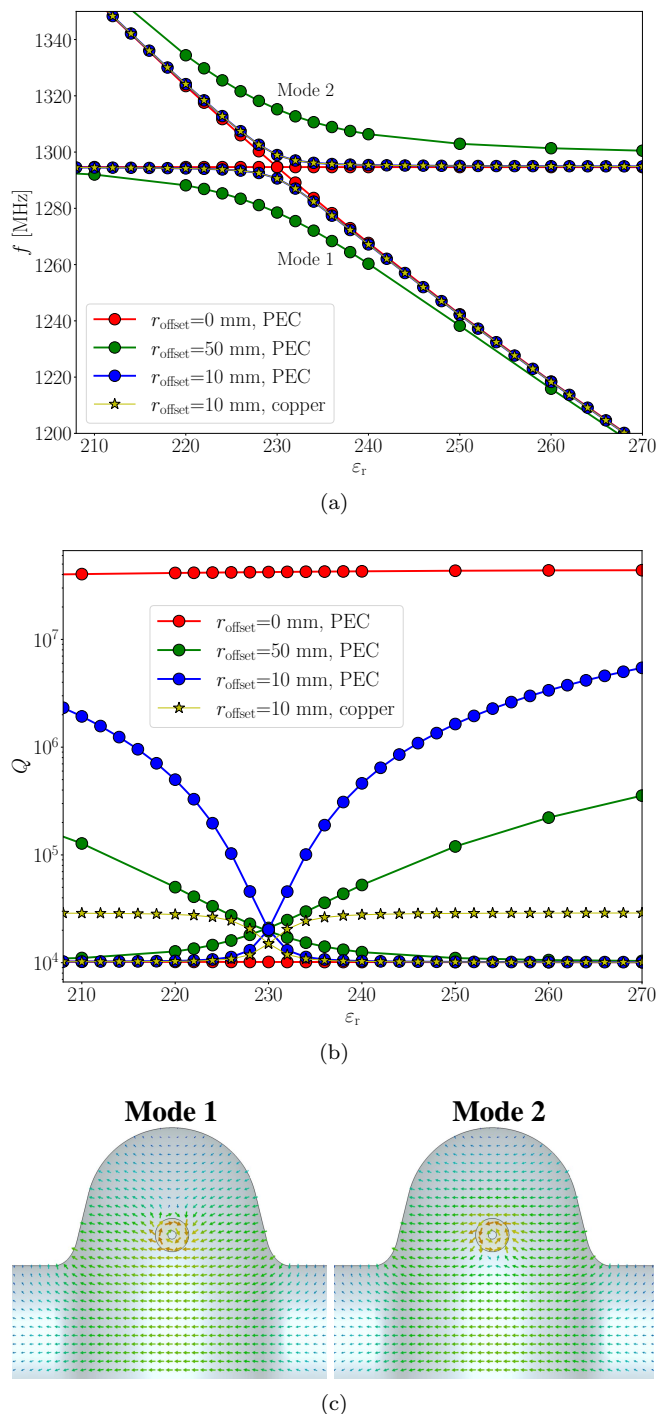


FIG. 5. Parameter sweep of the dielectric constant (ϵ_r) of STO and its effect on the frequency and quality factor of the first two modes of the coupled elliptical cavity and STO puck at different radial offset (r_{offset}) values. Mode 1 is the mode with the lower frequency. (a) Frequency of the eigenmodes, (b) quality factor of the eigenmodes, and (c) E-field distributions of the two modes at $\epsilon_r = 230$ and $r_{\text{offset}} = 50$ mm.

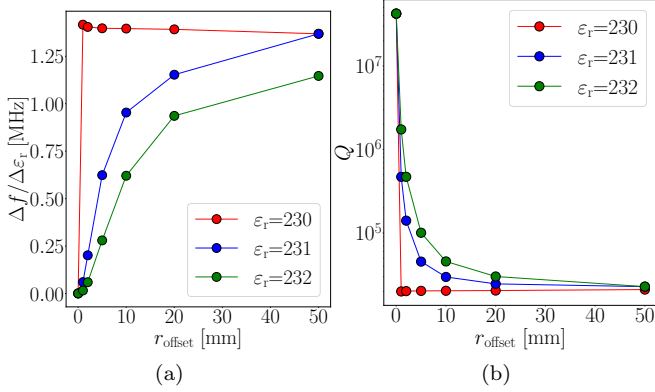


FIG. 6. Dependency of the frequency sensitivity (a) and quality factor (b) of the elliptical cavity-dominant mode with respect to r_{offset} at different values of ϵ_r .

respectively, for a PEC cavity. In this PEC situation, the Q -factor value is influenced by the losses in the dielectric region occupied by the STO puck. Conversely, the frequency of the STO-dominant mode decreases with increasing ϵ_r , while its Q -factor remains nearly constant at $Q_{\text{ext}} = 1.0 \times 10^4$. In this scenario, the frequencies of the elliptical cavity-dominant mode at 1.3 GHz and the STO-dominant mode are unaffected by each other and intersect at $\epsilon_r = 230$, with no interaction between the modes as ϵ_r changes (Fig. 5(a)). The permittivity value of 230 corresponds to a temperature above room temperature, even though the system is ideally intended for operation at lower temperatures where the STO's resonance frequency exhibits the greatest sensitivity to temperature variations (around 25 K). However, due to the fixed dimensions of the STO puck and the elliptical cavity's frequency, we adjust the STO permittivity to shift its resonance frequency near 1.3 GHz to investigate the mode coupling between the two resonators. Alternative dielectrics having low temperature permittivity values closer to those considered in the simulations were also considered. In particular, a rutile puck having similar dimensions shows, at 0.8 K, a mode at 2.6 GHz with Q -factor of 5.6×10^5 [42]. However the variation of the permittivity of rutile as a function of temperature is less marked [43], thus coupled resonator systems based on rutile resonators are expected to be less sensitive as bolometers.

When the STO puck is radially offset, mode splitting occurs at $\epsilon_r = 230$, and the interaction between the two modes intensifies as the radial offset increases from zero. The level repulsion, defined as the distance between the two dispersion curves, grows with larger radial offsets, indicating stronger coupling between the two modes (Fig. 5(a)). This coupling causes the Q -factor of the STO-dominant mode (low- Q mode) to increase, while the Q -factor of the elliptical cavity-dominant mode (high- Q mode) decreases, and both converge at $\epsilon_r = 230$ (Fig. 5(b)). For a PEC elliptical cavity and an STO puck

with $r_{\text{offset}}=50$ mm and $\epsilon_r = 230$, the two modes exhibit equal quality factors of approximately $Q = 2 \times 10^4$. One mode has a frequency of 1279 MHz, while the other is at 1315 MHz. The field plots for these two modes are presented in Fig. 5(c). In addition to changes in ϵ_r , the eigenmode frequency sensitivities and their quality factors also depend on the radial offset. As shown in the Fig. 6, at $\epsilon_r = 230$, where the coupling is at its maximum, even a slight radial offset of the puck results in a sharp reduction in the quality factor of the elliptical cavity-dominant mode. This is followed by an increase in the mode's frequency sensitivity to changes in ϵ_r .

In practice, eigenmode information is obtained through S-parameter measurements. Figure 7 illustrates the S-parameters for an excitation scheme using two antennas (as shown in Fig. 4), with a puck offset of 50 mm. Two key parameters in the measurement are the frequency sensitivity of the modes to variations in ϵ_r and the Q -factor of the modes. The quality factor can be calculated using a 3 dB method and is also related to phase variations in the $S_{1,2}$ curve; larger phase changes (i.e., a steeper phase derivative) correspond to a higher Q -factor. Using the phase derivative offers the benefit of not only analyzing the peaks but also assessing the sensitivity of the transmission zero. This notch, located between two resonance peaks in the S-parameters, corresponds to a point of minimal signal transmission.

Figure 7(c) illustrates the phase derivatives of the PEC cavity at various values of ϵ_r . The distribution or pattern of the phase derivative near resonance frequencies exhibits a Lorentzian shape. For modes near 1.3 GHz (corresponding to the elliptical cavity's dominant mode), the phase derivative amplitude shows high values, indicating a large Q -factor. For the notch mode, the phase derivative peak remains nearly constant across different values of ϵ_r . For a normal conducting cavity, such as copper, the S-parameters are similar; however, the phase derivative amplitudes at the peaks are smaller, indicating a lower Q -factor.

Figure 8 presents the frequencies of the two peaks in the $S_{1,2}$ curve, along with the notch between them. The resonance behavior as a function of ϵ_r resembles eigenmode analysis, with level repulsion influenced by the r_{offset} . The frequency of the notch shifts similarly to that of the single STO puck calculated from the semi-analytical formula Eq. 1. The frequency sensitivity of modes 1 and 2 is generally lower than that of the notch as shown in Fig. 8(b). Similar to the eigenmode analysis, for ϵ_r below 230, mode 1 is the elliptical cavity-dominant mode, whereas above 230, it becomes the second mode. For the elliptical cavity-dominant mode, frequency sensitivity peaks at $\epsilon_r = 230$, although this is accompanied by a decrease in its phase derivative amplitude that is related to Q -factor value. However, the product of frequency sensitivity and the phase derivative for the two modes is equal to that of the notch for a PEC cavity (Fig. 8(c)), whereas for a copper cavity (Fig. 8(d)), this product for the notch exceeds that of the two modes.

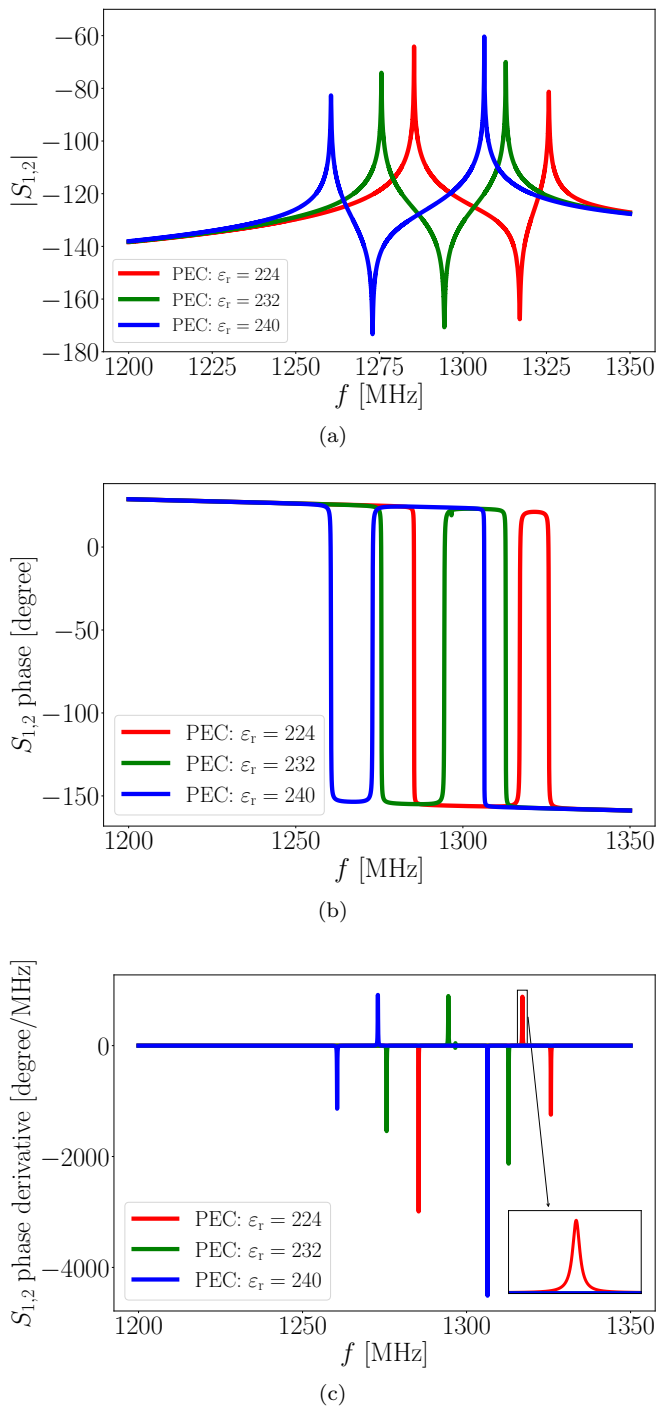


FIG. 7. S-parameters of the excitation scheme shown in Fig. 4 at different ϵ_r and $r_{\text{offset}} = 50$ mm for a PEC cavity. (a) Magnitude of $S_{1,2}$, (b) Phase (φ) of $S_{1,2}$, and (c) Phase derivative ($d\varphi/df$) of $S_{1,2}$. Varying ϵ_r shifts the resonance frequencies of the two peaks and the notch. The phase derivative is linked to the quality factor, with higher amplitude for the mode with the larger Q -factor, and shows minimal change at the notch as ϵ_r varies.

This coupling allows for a trade-off between higher frequency sensitivity and a higher Q -factor, depending on

the ϵ_r value.

Test measurements. To assess the coupling between the two modes in practice, a test case was established by placing the STO puck inside an elliptical cavity. Excitation is provided through two long rods positioned at the end flanges, and the STO puck is secured at the center of the cavity with a radial offset of 19 mm, mounted on a ceramic rod (see Fig. 9). The resonance of the STO puck, observed at 1.16 GHz in Fig. 9(b), is consistent with the predictions of the simulations, corroborating the analysis reported in this section. In addition to the fundamental mode of the STO puck and the elliptical cavity, many other higher-order modes can also be excited in the resonators, which are partially reproduced by the simulated model (Fig. 9(c)). Depending on the application, one or more of these modes with different frequencies, field patterns, and frequency sensitivities could also be selected for mode coupling.

IV. DISCUSSION

Unlike the power detection scheme, the fundamental limit in frequency measurements comes from the best achievable frequency stability of the measurement parts and thus it is not directly related to the Nyquist noise and the ambient temperature, although cryogenic cooling may significantly improve the detection limit by increasing the quality factors. By using superconducting cavities and sapphire, it is possible to achieve Q -factors in the 10^9 range [44] and bandwidths of the order of 1 Hz at microwave frequencies [45, 46]. This, also considering that the resolution of the resonator linewidth is typically limited, by electronic noise, to about 1 ppm [44], explains the unprecedented sensitivity of the frequency measurement approach.

By conjugating the frequency sensitivity of the high- Q cavity and the tunability introduced by coupling it with the STO resonator (Sec. III), we can envisage the possible use of the hybrid system in sensing applications. Although the specific characteristics of a particular sensor depends by its geometry and working conditions, we can anticipate the potentialities of the proposed hybrid system in this context. In particular, coupled dielectric resonators have already been proposed for the realization of sensitive particle and radiation bolometers at frequency around 10 GHz. In the bolometer detector described in Ref. [12, 20–22, 47], two resonators, realized using Sapphire and STO pucks, are positioned one on the top of the other and coupled by fringing fields. In the weak coupling regime, the maximum sensitivity to frequency occurs when the frequency of the two resonators exactly coincides and [47]

$$\left. \frac{df(T)}{dT} \right|_{\text{max}} = \frac{A}{(W_{\text{STO}})^2} \frac{df_{\text{STO}}}{dT}, \quad (2)$$

being A the coefficient that accounts for the coupling between the resonators modes and W_{STO} the unperturbed

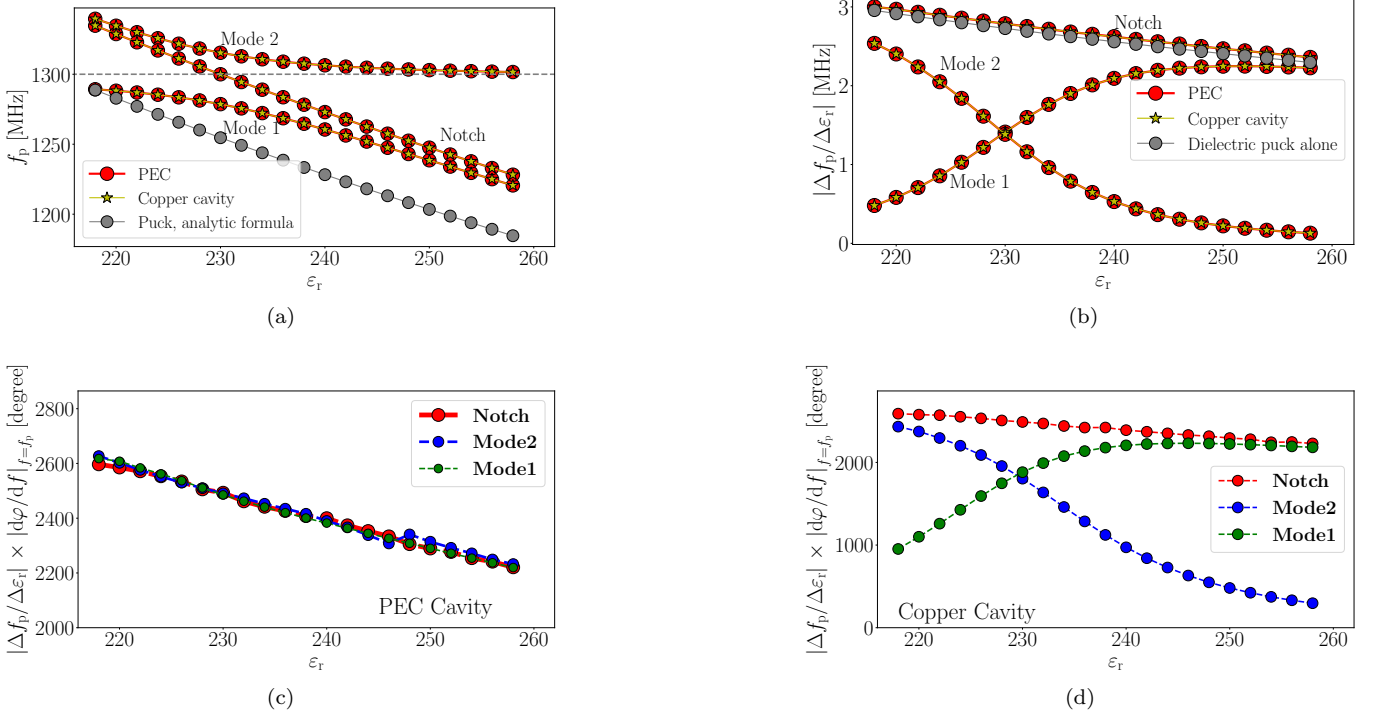


FIG. 8. Analysis of the S-parameters shown in Fig. 7. (a) Frequencies of the first and second peaks, as well as the notch, of the $|S_{1,2}|$ curves shown in Fig. 7(a). (b) Derivative of the curves from (a). (c) and (d) show the curves in (b) multiplied by the phase derivative at $f = f_p$ (from Fig. 7(c)), for a PEC cavity and a copper cavity, respectively. Mode 1 and Mode 2 correspond to the frequencies of the first and second peaks of the $|S_{1,2}|$ curves, respectively, and the notch corresponds to the frequency of the dip between these two peaks. The frequency of the puck alone and its derivative calculated by the semi-analytic formula is also shown in (a) and (b). The product of frequency sensitivity and the maximum phase derivative is almost equal at the notch for both the PEC and copper cavities (red curves in (c) and (d)). However, for modes 1 and 2, it is smaller in the copper cavity compared to the PEC cavity near ϵ_r of 230, where the coupling is at its maximum.

linewidth of STO [12]. The sensitivity of the bolometer is thus related to the temperature dependence of the frequency of the STO resonator (df_{STO}/dT). From Eq. 1 we obtain

$$\frac{df_{\text{STO}}}{dT} = -\frac{\alpha}{2} \epsilon_r^{-3/2} \frac{d\epsilon_r}{dT}, \quad (3)$$

being α related to the dimensions of the STO puck. Eq. 2 shows that the maximum sensitivity can be amplified by properly arranging the $A/(W_{\text{STO}})^2$ factor.

We focus here on the possibility to exploit the coupled cavity-STO resonator system as a bolometer, that is by replacing the originally proposed sapphire resonator with an elliptical cavity. The main advantages of this scheme are the possibility to tune the coupling strength by varying the STO puck position within the cavity and, in particular, to achieve higher couplings than those due to fringing fields of dielectric resonators positioned at a short distance [12]. As shown by electromagnetic simulations reported in Sec. III, the frequency sensitivity is quantified as $df/d\epsilon_r = 2.8$ MHz for $\epsilon_r \approx 230$. How this number is translated in df/dT sensitivity depends by the dimensions of the resonator and by the specific working conditions, in particular by the temperature range.

The temperature-dependence of the STO resonator frequency is not trivial owing to the structural transition around 100 K, the ferroelectric phase transition at 51 K and the stabilization of the quantum paraelectric phase below 5 K [35–37]. Let's first consider temperatures between 20 and 80 K, where the relative permittivity of STO can be approximated as $\epsilon_r \approx 10^5/T \approx 2000$. This range was discussed in the original proposal by Gallop et al. [12] and the frequency sensitivity quantified as $df(T)/dT = Af_0/(2W_{\text{STO}}^2 T)$. Considering the outcome of simulations reported in Sec. III, we expect that higher couplings enable the improvement of $df(T)/dT$ if the sapphire resonator is replaced by the metal cavity. Although the Q -factor of the normal-conducting cavity is typically lower than that of sapphire resonator [48], simulations suggest that, to obtain the maximum sensitivity, the change of the notch frequency should be considered (Fig. 8(d)).

We shall consider also the temperature range in which the cavity has superconducting properties. In particular, a Nb coated TESLA cavity is superconducting below 9.2 K where the Q -factor of the fundamental mode rises above 10^9 [40]. Ideally, when the superconducting cavity is cooled below the critical temperature, the STO puck

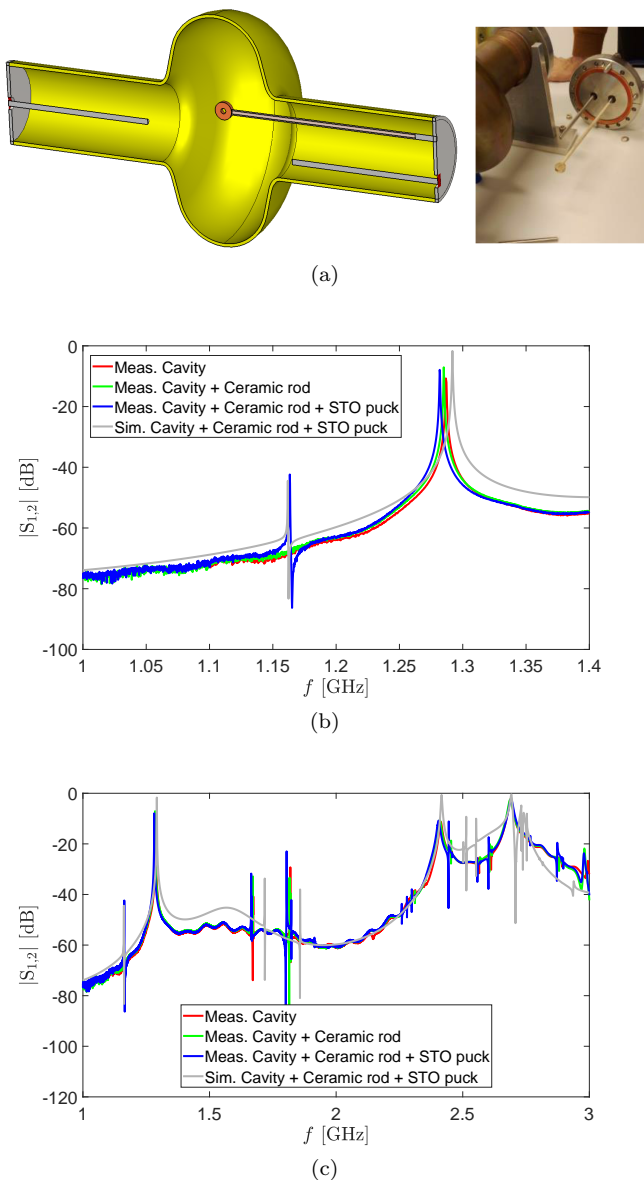


FIG. 9. The measurement setup (a) and measurement results of the coupled elliptical cavity with the STO puck over a narrow frequency range (b) and a wide frequency range (c). The STO puck is fixed to the flange via a long ceramic rod at $r_{\text{offset}}=19$ mm. Two long antennas were used for the $S_{2,1}$ measurement: one at the flange center and the other at $r_{\text{offset}}=-19$ mm. Note that the elliptical cavity used for the measurements had a slightly different shape than the one used for the simulations, causing a small change of the resonance modes of the cavity. An ϵ_r of 300 is assumed in the simulation.

should be warm up to $T \approx 25$ K to display the maximum value of df_{STO}/dT [22]. This requirement, however, introduces further experimental complexity. Fig. 2 shows that between 1 and 0.4 K the frequency of the STO resonator alone decreases monotonically with temperature; from the fit we derive $df_{\text{STO}}/dT = 10$ kHz/K at 0.8 K. This number is much smaller than what ob-

tained at $T \approx 20 - 25$ K [22], however it is expected to increase if small STO pucks are used (Eq. 3), as required, when the permittivity rises up to $\epsilon_r \approx 30000$, to match the frequencies of the STO resonator and cavity. Additionally, the hybrid system can be tuned to increase the coupling strength and compensate, at least partially, lower df_{STO}/dT values in this temperature range (Eq. 2). Given $\epsilon_r \approx 30000$, we expect that resonators having typical diameter in the range of 1 mm are needed to achieve a significant resonant coupling with the 1.3 GHz cavity. Considering that the heat capacity of the puck, which is directly related to the mass, plays a significant role in the system's effectiveness as a bolometer [47], we expect that reducing the puck's size increases sensitivity by amplifying the temperature rise per unit of absorbed energy, thereby enhancing the system's detection capabilities.

Given the very peculiar characteristic of STO and the dependence of the STO resonator frequency by external factors such as applied electric field or mechanical stress, we just mention that possible applications of the proposed system of coupled cavity and STO puck are not limited to the realization of bolometers. Simulations indicate that the two cavities can be tuned to reach the strong coupling regime (Fig. 5). As expected, at resonance the quality factor of the superconducting cavity progressively decreases as the coupling increases. However, we note that eigenmodes having Q -factor in the $10^5 - 10^6$ range can still be obtained by adjusting r_{offset} and the detuning of the natural frequencies of superconducting cavity and STO resonator. These values are corroborated by transmission spectra measured at low temperature (Fig. 2), which show that the Q -factor of the STO resonator is in the 10^4 range. This value can potentially be further improved by using opportunely prepared STO pucks. Electromagnetic simulations also show that the change of the frequency of the superconducting cavity modes location, and of the corresponding phase, are amplified as an effect of the coupling with the STO resonator (Fig. 7). In this regard, the phase derivative of $S_{1,2}$ shows a particularly steep response.

We also mention that preliminary tests were carried out to test the stability of the STO mode frequency. In the case of measurements running for hours, the observed drift of the resonance frequency, due to external factors and without any feedback control, was in the range of 50 Hz both for the STO puck measured at 0.1 K and for superconducting cavities measured at 1.7 K. These values are strongly reduced, of about one order of magnitude, for timescales of few seconds or minutes. By improving the experimental set up, and introducing a reference phase-locked loop (PLL) frequency stabilization, it is expected a significant reduction of the frequency drift, thus allowing to exploit phase measurements and further improve the system sensitivity. Additionally, the frequency tuning of the detection cavity can be ensured by the ferroelectricity of the STO and can be obtained by applying a DC electric field to the dielectric resonator. The expected tuning range is in the order of few percent.

V. CONCLUSIONS

To conclude, we have studied the hybrid system composed by a high- Q TESLA-shaped elliptical cavity and STO resonator, and investigated the effect of parameters, such as STO permittivity, puck dimensions and position within the cavity, that govern the coupling between the electromagnetic modes. Finite-element simulations show that the hybrid system offers great versatility to tune the coupling strength and achieve the strong coupling regime. These results are supported by test measurements carried out at room temperature using a copper cavity and a STO puck, and by the low temperature characterization of the STO resonator, which shows resonant frequency of 0.1 GHz and Q -factor of 10000 at 0.16 K. The hybrid system show potential for the realization of microwave sensors in which the sensitivity of the STO puck to selected physical quantities is exploited as the active element, while frequency or phase measure-

ments on the high- Q cavity are used to efficiently detect such changes. In particular, the application of the hybrid system in bolometers exploiting the temperature dependence of the STO permittivity has been discussed. Our results are useful to design dedicated experiments at low temperature allowing the direct test of sensitivity and tunability of the proposed hybrid system in high precision frequency-domain measurements.

VI. ACKNOWLEDGMENTS

We thank Fritz Casper, Sergio Calatroni, Akira Miyazaki, Walter Venturini, Alick Mcpherson, Giovanni Carugno and Marco Affronte for stimulating discussions. A.C. acknowledges financial support from PNRR MUR project E63C22002190007, PE23, NQSTI. A.G. acknowledges financial support from PNRR MUR project ECS_00000033.ECOSISTER. S.P. acknowledges financial support from PNRR MUR NQSTI PE000000023 project HIQRES CUP H43C22000870001.

-
- [1] S. Asztalos, G. Carosi, C. Hagmann, D. Kinion, K. van Bibber, M. Hotz, L. J. Rosenberg, G. Rybka, A. Wagner, J. Hoskins, C. Martin, N. Sullivan, D. Tanner, R. Bradley, and J. Clarke, Design and performance of the admx squid-based microwave receiver, *Nuclear Instruments and Methods in Physics Research Section A: Accelerators, Spectrometers, Detectors and Associated Equipment* **656**, 39 (2011).
- [2] N. Du, N. Force, R. Khatiwada, E. Lentz, R. Ottens, L. J. Rosenberg, G. Rybka, G. Carosi, N. Woollett, D. Bowring, A. S. Chou, A. Sonnenschein, W. Wester, C. Boutan, N. S. Oblath, R. Bradley, E. J. Daw, A. V. Dixit, J. Clarke, S. R. O’Kelley, N. Crisosto, J. R. Gleason, S. Jois, P. Sikivie, I. Stern, N. S. Sullivan, D. B. Tanner, and G. C. Hilton (ADMX Collaboration), Search for invisible axion dark matter with the axion dark matter experiment, *Phys. Rev. Lett.* **120**, 151301 (2018).
- [3] R. H. Parker, C. Yu, W. Zhong, B. Estey, and H. Muller, Measurement of the fine-structure constant as a test of the standard model, *Science* **360**, 191 (2018).
- [4] M. Nagel, S. R. Parker, E. V. Kovalchuk, P. L. Stanwix, J. G. Hartnett, E. N. Ivanov, A. Peters, and M. E. Tobar, Direct terrestrial test of lorentz symmetry in electrodynamics to 10^{-18} , *Nature Communications* **6**, 8174 (2015).
- [5] A. Lo, P. Haslinger, E. Mizrachi, L. Anderegg, H. Müller, M. Hohensee, M. Goryachev, and M. E. Tobar, Acoustic tests of lorentz symmetry using quartz oscillators, *Phys. Rev. X* **6**, 011018 (2016).
- [6] A. Blais, R.-S. Huang, A. Wallraff, S. M. Girvin, and R. J. Schoelkopf, Cavity quantum electrodynamics for superconducting electrical circuits: An architecture for quantum computation, *Phys. Rev. A* **69**, 062320 (2004).
- [7] M. Reagor, W. Pfaff, C. Axline, R. W. Heeres, N. Ofek, K. Sliwa, E. Holland, C. Wang, J. Blumoff, K. Chou, M. J. Hatridge, L. Frunzio, M. H. Devoret, L. Jiang, and R. J. Schoelkopf, Quantum memory with millisecond coherence in circuit qed, *Phys. Rev. B* **94**, 014506 (2016).
- [8] S. Barzanjeh, M. Wulf, M. Peruzzo, M. Kalaei, P. B. Dieterle, O. Painter, and J. M. Fink, Mechanical on-chip microwave circulator, *Nature Communications* **8**, 953 (2017).
- [9] B. J. Bloom, T. L. Nicholson, J. R. Williams, S. L. Campbell, M. Bishof, X. Zhang, W. Zhang, S. L. Bromley, and J. Ye, An optical lattice clock with accuracy and stability at the 10^{-18} level, *Nature* **506**, 71 (2014).
- [10] D. G. Matei, T. Legero, S. Häfner, C. Grebing, R. Weyrich, W. Zhang, L. Sonderhouse, J. M. Robinson, J. Ye, F. Riehle, and U. Sterr, 1.5 μm lasers with sub-10 mhz linewidth, *Phys. Rev. Lett.* **118**, 263202 (2017).
- [11] N. R. Newbury, Searching for applications with a fine-tooth comb, *Nature Photonics* **5**, 186 (2011).
- [12] J. Gallop and L. Hao, Applications of coupled dielectric resonators using srtio/sub 3/ pucks: tuneable resonators and novel thermometry, *IEEE Transactions on Instrumentation and Measurement* **50**, 526 (2001).
- [13] C. J. Axline, L. D. Burkhardt, W. Pfaff, M. Zhang, K. Chou, P. Campagne-Ibarcq, P. Reinhold, L. Frunzio, S. M. Girvin, L. Jiang, M. H. Devoret, and R. J. Schoelkopf, On-demand quantum state transfer and entanglement between remote microwave cavity memories, *Nature Physics* **14**, 705 (2018).
- [14] K. S. Chou, T. Shemma, H. McCarrick, T.-C. Chien, J. D. Teoh, P. Winkel, A. Anderson, J. Chen, J. C. Curtis, S. J. de Graaf, J. W. O. Garmon, B. Gudlewski, W. D. Kalfus, T. Keen, N. Khedkar, C. U. Lei, G. Liu, P. Lu, Y. Lu, A. Maiti, L. Mastalli-Kelly, N. Mehta, S. O. Mundhada, A. Narla, T. Noh, T. Tsunoda, S. H. Xue, J. O. Yuan, L. Frunzio, J. Aumentado, S. Puri, S. M. Girvin, S. H. Moseley, and R. J. Schoelkopf, A superconducting dual-rail cavity qubit with erasure-detected logical measurements, *Nature Physics* 10.1038/s41567-024-

- 02539-4 (2024).
- [15] A. Majumdar, M. Bajcsy, A. Rundquist, and J. Vučković, Loss-enabled sub-poissonian light generation in a bimodal nanocavity, *Phys. Rev. Lett.* **108**, 183601 (2012).
- [16] C. Wang, Y.-L. Liu, R. Wu, and Y.-x. Liu, Phase-modulated photon antibunching in a two-level system coupled to two cavities, *Phys. Rev. A* **96**, 013818 (2017).
- [17] C. Bonizzoni, F. Troiani, A. Ghirri, and M. Affronte, Microwave dual-mode resonators for coherent spin-photon coupling, *Journal of Applied Physics* **124**, 194501 (2018).
- [18] C. Wang, O. S. Melnychuk, C. Contreras-Martinez, Y. Lu, Y. M. Pischalnikov, O. Pronitchev, B. Giaccone, R. Pilipenko, S. Zorzetti, S. Posen, A. Romanenko, and A. Grassellino, Phase-controlled improvement of photon lifetime in coupled superconducting cavities, *Phys. Rev. Appl.* **21**, 024040 (2024).
- [19] B. T. McAllister, G. Flower, L. E. Tobar, and M. E. Tobar, Tunable supermode dielectric resonators for axion dark-matter haloscopes, *Phys. Rev. Appl.* **9**, 014028 (2018).
- [20] L. Hao, J. Gallop, and J. Macfarlane, Coupled microwave resonators for sensitive bolometric detection, *IEEE Transactions on Instrumentation and Measurement* **54**, 886 (2005).
- [21] L. Hao, T. Quincey, G. Lorusso, J. Keightley, J. Chen, and J. Gallop, Sensitive calorimeter based on coupled dielectric resonators, in *2020 Conference on Precision Electromagnetic Measurements (CPEM)* (2020) pp. 1–3.
- [22] L. Hao, G. Lorusso, and J. C. Gallop, Coupled resonator calorimeter for particle detection, *IEEE Transactions on Instrumentation and Measurement* **70**, 1 (2021).
- [23] H. Wang and Q.-X. Chu, Generation of transmission zero through electric and magnetic mixed coupling, in *2007 International Conference on Microwave and Millimeter Wave Technology* (2007) pp. 1–3.
- [24] L. Su, J. Mata-Contreras, P. Velez, and F. Martin, A review of sensing strategies for microwave sensors based on metamaterial-inspired resonators: Dielectric characterization, displacement, and angular velocity measurements for health diagnosis, telecommunication, and space applications, *International Journal of Antennas and Propagation* **2017**, 5619728 (2017).
- [25] J. Breeze, K.-J. Tan, B. Richards, J. Sathian, M. Oxborrow, and N. M. Alford, Enhanced magnetic purcell effect in room-temperature masers, *Nature Communications* **6**, 6215 (2015).
- [26] P. Brun, A. Caldwell, L. Chevalier, G. Dvali, P. Freire, E. Garutti, S. Heyminck, J. Jochum, S. Knirck, M. Kramer, C. Krieger, T. Lasserre, C. Lee, X. Li, A. Lindner, B. Majorovits, S. Martens, M. Matysek, A. Millar, G. Raffelt, J. Redondo, O. Reimann, A. Ringwald, K. Saikawa, J. Schaffran, A. Schmidt, J. Schütte-Engel, F. Steffen, C. Strandhagen, G. Wieching, and M. Collaboration, A new experimental approach to probe qcd axion dark matter in the mass range above 40 eV , *The European Physical Journal C* **79**, 186 (2019).
- [27] E. R. Eisenach, J. F. Barry, M. F. O’Keeffe, J. M. Schloss, M. H. Steinecker, D. R. Englund, and D. A. Braje, Cavity-enhanced microwave readout of a solid-state spin sensor, *Nature Communications* **12**, 1357 (2021).
- [28] H. H. Vallabhapurapu, J. P. Slack-Smith, V. K. Sewani, C. Adambukulam, A. Morello, J. J. Pla, and A. Laucht, Fast coherent control of a nitrogen-vacancy-center spin ensemble using a ktao₃ dielectric resonator at cryogenic temperatures, *Phys. Rev. Appl.* **16**, 044051 (2021).
- [29] Y.-Y. Pai, A. Tylan-Tyler, P. Irvin, and J. Levy, Physics of srtio₃-based heterostructures and nanostructures: a review, *Reports on Progress in Physics* **81**, 036503 (2018).
- [30] R. A. Cowley, Lattice dynamics and phase transitions of strontium titanate, *Phys. Rev.* **134**, A981 (1964).
- [31] K. A. Müller and H. Burkard, SrTiO₃: An intrinsic quantum paraelectric below 4 k, *Phys. Rev. B* **19**, 3593 (1979).
- [32] R. Viana, P. Lunkenheimer, J. Hemberger, R. Böhmer, and A. Loidl, Dielectric spectroscopy in srTiO₃, *Phys. Rev. B* **50**, 601 (1994).
- [33] J. F. Schooley, W. R. Hosler, and M. L. Cohen, Superconductivity in semiconducting srTiO₃, *Phys. Rev. Lett.* **12**, 474 (1964).
- [34] X. Wang, A. Kundu, B. Xu, S. Hameed, N. Rothen, S. Rabkin, L. Rogić, L. Thompson, A. McLeod, M. Greven, D. Pelc, I. Sochnikov, B. Kalisky, and A. Klein, Multiferroicity in plastically deformed srTiO₃, *Nature Communications* **15**, 7442 (2024).
- [35] R. G. Geyer, B. Riddle, J. Krupka, and L. A. Boatner, Microwave dielectric properties of single-crystal quantum paraelectrics KTaO₃ and SrTiO₃ at cryogenic temperatures, *Journal of Applied Physics* **97**, 104111 (2005).
- [36] M. A. Hosain, J.-M. Le Floch, J. F. Bourhill, J. Krupka, M. E. Tobar, Ferroelectric phase transition and crystal asymmetry monitoring of SrTiO₃ using quasi TEm_{1,1} and quasi TMm_{1,1} modes, *Journal of Applied Physics* **126**, 104102 (2019).
- [37] Z. C. Zhao, M. Goryachev, J. Krupka, and M. E. Tobar, Precision multi-mode dielectric characterization of a crystalline perovskite enables determination of the temperature-dependent phase transitions, *IEEE Transactions on Ultrasonics, Ferroelectrics, and Frequency Control* **69**, 423 (2022).
- [38] D. Davidovikj, N. Manca, H. S. J. van der Zant, A. D. Caviglia, and G. A. Steele, Quantum paraelectricity probed by superconducting resonators, *Phys. Rev. B* **95**, 214513 (2017).
- [39] V. T. Engl, N. G. Ebensperger, L. Wendel, and M. Scheffler, Planar ghz resonators on srTiO₃: Suppressed losses at temperatures below 1 k (2019), arXiv:1911.11456 [cond-mat.supr-con].
- [40] B. Aune, R. Bandelmann, D. Bloess, B. Bonin, A. Bosotti, M. Champion, C. Crawford, G. Deppe, B. Dwersteg, D. A. Edwards, H. T. Edwards, M. Ferrario, M. Fouaidy, P.-D. Gall, A. Gamp, A. Gössel, J. Graber, D. Hubert, M. Hüning, M. Juillard, T. Junquera, H. Kaiser, G. Kreps, M. Kuchnir, R. Lange, M. Leenen, M. Liepe, L. Lilje, A. Matheisen, W.-D. Möller, A. Mosnier, H. Padamsee, C. Pagani, M. Pekeler, H.-B. Peters, O. Peters, D. Proch, K. Rehlich, D. Reschke, H. Safa, T. Schilcher, P. Schmüser, J. Sekutowicz, S. Simrock, W. Singer, M. Tigner, D. Trines, K. Twarowski, G. Weichert, J. Weisend, J. Wojtkiewicz, S. Wolff, and K. Zapfe, Superconducting tesla cavities, *Phys. Rev. ST Accel. Beams* **3**, 092001 (2000).
- [41] D. Kajfez and P. Guillon, *Dielectric Resonators*, Artech House microwave library (Noble Publishing Corporation, 1998).
- [42] A. Cassinese, to be published.

- [43] R. A. Parker, Static dielectric constant of rutile (TiO_2), 1.6-1060°k, *Phys. Rev.* **124**, 1719 (1961).
- [44] A. G. Mann, Ultrastable cryogenic microwave oscillators, in *Frequency Measurement and Control, Topics in Applied Physics*, edited by A. N. Luiten (Springer Berlin, Heidelberg, 2001).
- [45] Y. Pischalnikov, D. Bice, A. Grassellino, T. Khabiboulline, O. Melnychuk, R. Pilipenko, S. Posen, O. Pronitchev, and A. Romanenko, Operation of an srf cavity tuner submerged into liquid he, in *Proc. SRF'19, International Conference on RF Superconductivity No. 19* (JACoW Publishing, Geneva, Switzerland, 2019) pp. 660–663.
- [46] A. Romanenko, R. Harnik, A. Grassellino, R. Pilipenko, Y. Pischalnikov, Z. Liu, O. S. Melnychuk, B. Giaccone, O. Pronitchev, T. Khabiboulline, D. Frolov, S. Posen, S. Belomestnykh, A. Berlin, and A. Hook, Search for dark photons with superconducting radio frequency cavities, *Phys. Rev. Lett.* **130**, 261801 (2023).
- [47] L. Hao, J. Gallop, and J. Macfarlane, Coupled microwave resonators as the basis for sensitive bolometric detection, *IEEE Transactions on Instrumentation and Measurement* **52**, 328 (2003).
- [48] R. Di Vora, D. Alesini, C. Braggio, G. Carugno, N. Crescini, D. D'Agostino, D. Di Gioacchino, P. Falferi, U. Gambardella, C. Gatti, G. Iannone, C. Ligi, A. Lombardi, G. Maccarrone, A. Ortolan, R. Pengo, A. Rettaroli, G. Ruoso, L. Taffarello, and S. Tocci, High- q microwave dielectric resonator for axion dark-matter haloscopes, *Phys. Rev. Appl.* **17**, 054013 (2022).